Journal of Applied Electrochemistry **29**: 927–937, 1999.

Zn and Zn–Sn alloy coatings with and without chromate layers. Part I: Corrosion resistance and structural analysis

L. SZIRÁKI[1]*, Á. CZIRÁKI[2], Z. VÉRTESY[3], L. KISS[1], V. IVANOVA[4], G. RAICHEVSKI[4], S. VITKOVA[4], S. and Ts. MARINOVA[5]

[1]*Department of Physical Chemistry, Eötvös L. University, H-1518 Budapest 112, PO Box 32, Hungary*
[2]*Department of Solid State Physics, Eötvös L. University, H-1088 Budapest, Múzeum krt.6-8., Hungary*
[3]*Research Institute for Materials Sciences, Hungarian Academy of Science, H-1525 Budapest, PO Box 49, Hungary*
[4]*Institute of Physical Chemistry, Bulgarian Academy of Science, Sofia 1040, Bulgaria*
[5]*Institute of General and Inorganic Chemistry, Bulgarian Academy of Science, Sofia 1040, Bulgaria*
*(*author for correspondence, e-mail: sziraki@ludens.elte.hu)*

Received 19 May 1998; accepted in revised form 8 December 1998

Key words: conversion coatings, EIS, TEM, XPS, Zn corrosion, Zn–Sn alloy corrosion

Abstract

The aqueous corrosion resistances of Zn and Zn–Sn (~20 wt % Sn) electrodeposits, passivated by immersion in chromating solution with different ratios of Cr(VI) to activating ions, are compared. The electrochemical behaviour of various chromated and nonchromated coatings were investigated in deaerated 0.5 mol dm^{-3} Na_2SO_4/pH 5 solution using a.c. impedance and d.c. polarization techniques. The polarization curves revealed that the chromate layers influence both the cathodic and anodic reactions. The corrosion rate of each specimen decreases with time due to the accumulation of corrosion products. The dark yellow (DY) chromate film on the Zn–Sn alloy and the iridiscent yellow (IY) on Zn yields the best protective ability in agreement with the assessment of prolonged salt spray chamber tests. These chromate layers resembling cracked mud become permeable to the electrolyte after immersion and, as a consequence of the transformation and the leaching of certain Cr compounds, a very porous agglomerate of corrosion products forms. The morphology and structure of dark yellow chromated Zn–Sn alloy was also investigated by transmission electromicroscopy (TEM) and scanning electronmicroscopy with microprobe (SEM/EDS) analyses before and after corrosion. The depth profile of the corroded surface chemical composition was determined by X-ray photoelectron spectroscopy (XPS).

1. Introduction

Chemical chromating is often used to enhance the corrosion stability and/or paint adhesion of Zn plates or galvanized steel. The active/passive type of corrosion behaviour observed on Zn–Sn alloy with 0 – 80 wt % tin content [1] is also expected to be improved by chromating. The thermal Zn–Sn alloy with tin content up to 80% is sacrificial to steel in slightly acidic and neutral salt solution [1], because zinc maintains the corrosion potential at a more negative value than does pure tin but the Zn loss from the alloy is moderated by the the accumulated porous zinc and tin oxides. The corrosion resistance of the Zn–Sn alloy strongly depends on its composition and the corrosion medium. Although the corrosion resistance of the Zn–Sn alloy is not actually lower than that of pure Zn, Sn or Cd, it is often used as an alternative for these metals from various practical and economical considerations [2–5]. Earlier we reported a series of studies on these problems. Zn–Sn alloy coatings containing 10–30% tin were deposited from a slightly acid electrolyte and the deposition conditions were optimized [6]. We proposed three compositions with appropriate Cr(VI) activating ion ratios for chromating of electrodeposited Zn–Sn alloys with low Sn content. The results [7] of the accelerated electrochemical Paatsch test and a salt spray chamber test indicated an increasing protective ability of the chromate films in the following sequence: colourless (CL) on Zn–Sn > iridiscent yellow (IY) on

Zn–Sn > IY on Zn > dark yellow (DY) on Zn > DY on Zn–Sn. The better protective ability of the dark yellow chromate film on Zn–Sn and that of the iridiscent yellow on a Zn coating were related to the uniform corrosion of these microcracked conversion layers. The elemental and chemical compositions of some types of chromate passive film on Zn–Sn and Zn coatings were determined on the surface and in the depth by X-ray photoelectron spectroscopy (XPS) [8]. The film thickness was found to increase from the colourless through iridiscent yellow to uniformly coloured dark yellow chromate film. It was shown that besides chromium compounds, Zn and Sn corrosion products were present in the films.

The aim of the present study was to characterise the corrosion of Zn–Sn ($\sim$20 wt % Sn) coatings in the presence and absence of chromate layer in deaerated 0.5 mol dm^{-3} Na_2SO_4/pH 5 solution using d.c. polarization techniques and electrochemical impedance spectroscopy. We addressed the question whether protective ability of Zn–Sn coatings were more promising than that for pure Zn deposits. We also characterized the protection action of high performance chromate films.

To give a comprehensive kinetic/structural/compositional explanation for the prime protection ability of the dark yellow chromated Zn–Sn coating the electrochemical examination were completed with TEM, SEM and XPS analyses.

2. Experimental details

Zn and Zn–Sn alloy coatings of $\sim$10 μm were obtained on copper discs in an industrial acidic sulphate bath containing different addivites [6]. The coatings were chromated by immersion of the coated samples in the bath (Table 1). The corrosion medium was 0.5 mol dm^{-3} Na_2SO_4 solution (analytical grade) deaerated by continuous bubbling of argon gas through the solution at room temperature. The pH of the solution was adjusted to 5 by addition of H_2SO_4 solution.

A Tacussel EDI 101T assembly was used for electrode rotation. Unlike the nonchromated Zn and Zn–Sn deposits the electrode rotation rate had a slight effect on the polarization resistance (R_p) of the chromated samples. For this reason all measurements were conducted at a rotation rate of 1000 rpm.

Each type of electrochemical measurements was repeated 3–5 times on different samples and typical results are presented. A saturated calomel electrode (SCE) was used throughout as reference. The d.c. polarization measurements were performed using an AFKEL 450 (Hungary) PC controlled potentiostat.

The small amplitude EIS measurements were carried out using a Solartron 1250 frequency response analyser coupled to a 1286 electrochemical interface. To reduce the high frequency impedance of the reference electrode loop, a tap-free Luggin probe was employed whose tip was immersed below the solution surface. The impedance spectra were recorded in the frequency range 51 kHz to 10 mHz. The amplitude of the perturbing signal was 3 mV. The kinetic constants (Tafel slopes) of the coupled corrosion processes were determined by the potentiostatic faradaic distortion method [9] at the corrosion potential in those cases when the low frequency impedance attained the real axis limit, that is, the low frequency electrode capacitance became negligible.

The morphological observations of the samples were made using a Jeol 840 scanning electron microscope in the secondary electron imaging (SEI) mode.

The microanalysis of the samples was performed using an energy dispersive X-ray spectrometer (EDS). The measurements were carried out on an ORTEC System 5000 equipped with a Si(Li) detector with a Be window, which permits measurement of the elements from Na to U. The excitation depth was about 3.5 μm.

The microstructure of corrosion layers was characterized by TEM using a Philips CM20 microscope operated at 200 kV and equipped with an X-ray microanalysis facility (EDAX system). Cross-sectional samples for the TEM studies were prepared by ultramicrotome.

The XPS analysis of the samples was carried out in an ESCALAB Mk II (VG Scientific) electron spectrometer at base pressures in the preparation and analysis chambers of 2×10^{-8} and 1×10^{-8} Pa, respectively. The

Table 1. Composition of the chromating solutions taken from [6]

Samples	Appearance	Ratios of Cr(VI) to activating ions				
		Cr^{VI}/Cr^{III}	Cr^{VI}/SO_4^{2-}	Cr^{VI}/PO_4^{3-}	$Cr^{VI}/B_4O_7^{2-}$	Cr^{VI}/NO_3^-
Zn CL	Colourless	1.0–1.56	0.12–0.15	–	–	0.007–0.010
Zn IY	Iridiscent yellow	–	3.20	–	8.64	–
Zn DY	Dark yellow	–	0.62	3.0	–	–
Zn–Sn CL	Colourless	–	3.82	–	6.5	–
Zn–Sn DY	Dark yellow	–	1.60	8.3	–	–

photoelectrons were excited by an X-ray source using AlK_α ($h\nu = 1486.6$ eV). The instrumental resolution measured as the full width at half maximum (FWHM) of the Ag $3d_{5/2}$ photoelectron peak was 1.3 eV for a pass energy in the analyser of 20 eV. The C ls, O ls, P 2p, S 2p, Cr 2p, Zn 2p and Sn 3d photoelectron peaks were recorded. The intensities (I) were determined as the integrated peak areas assuming the background to be linear. The element concentrations were calculated by the SSI (Surface Science Instruments) approach taking the transmission function of the analyser into account [10]. The values of the respective cross section were taken from [11]. Depth profiling was carried out by sputtering at 45° using an argon beam of 3 keV and a current density of 10 μA cm^{-2}. The sputtering rate for this ion energy was about 1.5 nm min^{-1}.

3. Results and discussion

3.1. *Corrosion resistance of nonchromated and chromated Zn and Zn–Sn coatings in deaerated 0.5 mol dm^{-3} Na_2SO_4 solution*

Figures 1 and 2 show the effect of chromating on the polarization behaviour of Zn and Zn–Sn (~ 20 wt % Sn). The anodic and cathodic polarization curves are shifted toward lower rates approximately parallel to those of the nonchromated curves and the oxide reduction peaks of the corrosion products are also inhibited by chromating. This behaviour points to the presence of a porous barrier layer. Additionally, the enhanced shift of the anodic curve in the positive direction and the higher current of the cathodic plateau before the reduction peaks, observed after a more prolonged exposure (2′a and 2′k on Figure 2.), show that the increasing amount of corrosion products on dark yellow chromated Zn–Sn deposit preserves corrosion protection ability. In contrast, the colourless chromate layer on Zn which formed in a Cr(III)/Cr(VI) bath containing NO_3^- activating ion promotes zinc corrosion. Therefore, the polarization resistance measured at the corrosion potential either by d.c. or a.c. methods can be related to the coupled zinc dissolution and hydrogen evolution reactions.

Figures 3 and 4 show the complex plane plots of the impedance diagrams obtained on the corroding deposits. For the nonchromated and the colourless chromate coatings, two capacitive loops were observed, while the other passivated deposits showed a very complex response. In these cases the capacitive loops are expanded along the real axis indicating overlapping of a number of time constants. For the chromated samples the HF resistance corresponding to the combination of the solution and film resistance remained within 1–5% of the LF polarization resistance indicating either a conductive or a solution filled layer. The kinetic evaluation of the EIS diagrams will be examined in detail in the second part of the paper. For each type of deposit the impedance approached the real axis at low frequency, except for the colourless Zn–Sn and the dark yellow alloy at prolonged exposure. In the latter case we approximated the polar-

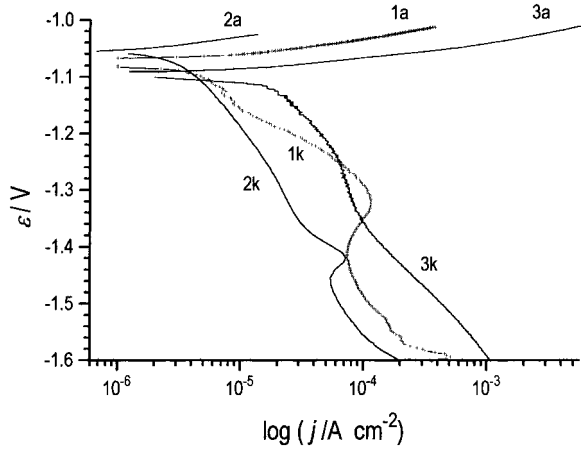

Fig. 1. Anodic and cathodic potentiodynamic polarization curves of Zn deposits with and without chromate layers after immersion into deaerated 0.5 mol dm^{-3} Na_2SO_4 solution/pH 5. Scan rate, $v = 10^{-3}$ V s^{-1}, $f = 1000$ rpm, corrosion time 1.5 h. Key: (1a, 1k) on bright Zn deposit; (2a, 2k) on Zn with iridiscent yellow chromate layer; (3a, 3k) on Zn with colourless chromate layer.

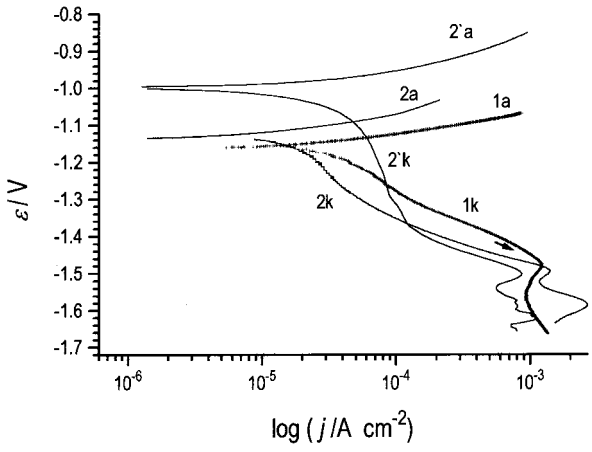

Fig. 2. Anodic and cathodic potentiodynamic polarization curves of ZnSn (20 wt % Sn) deposits with and without chromate layers after immersion in deaerated 0.5 mol dm^{-3} Na_2SO_4 solution/pH 5. Scan rate, $v = 10^{-3}$ V s^{-1}, $f = 1000$ rpm Key: (1a, 1k) on Zn–Sn, corrosion time 1.5 h; (2, 2′a, 2, 2′k) on Zn–Sn (20 wt % Sn) deposit with dark yellow chromate layer, corrosion time (2) 1.5 h, (2′) 52 h.

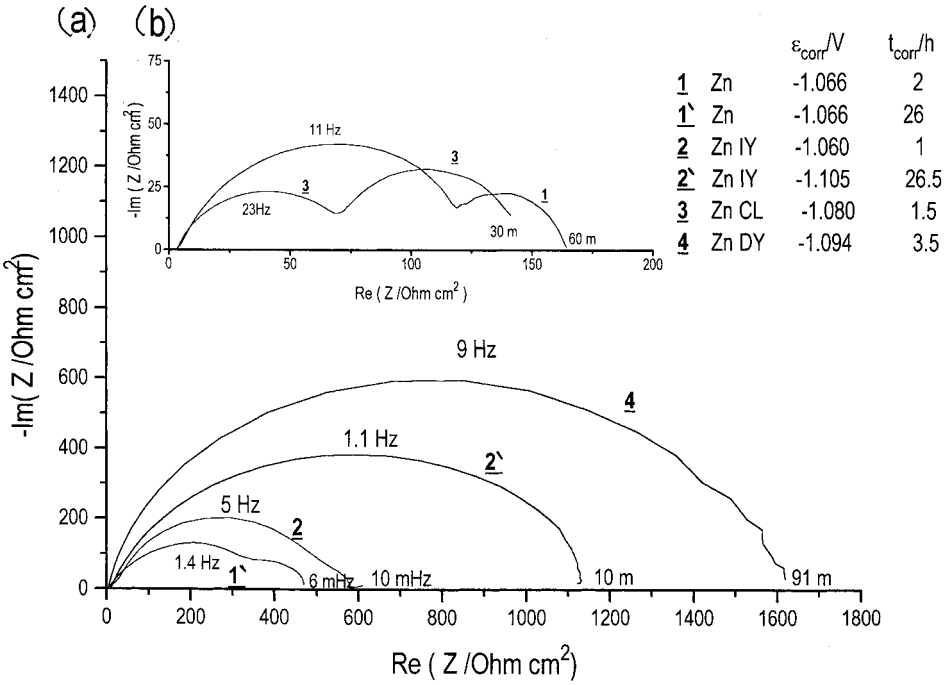

Fig. 3. Complex plane plots of measured impedance spectra of Zn deposits with and without chromate layers after immersion into deaerated 0.5 mol dm^{-3} Na_2SO_4 solution/pH = 5, f = 1000 rpm. Inset (a) (1′) Zn, t_{corr} = 26 h, (2, 2′) iridiscent yellow chromate on Zn, t_{corr} = 1 and 26.5 h, respectively, (4) dark yellow chromate on Zn, t_{corr} = 3.5 h. Inset (b) 1 Zn, t_{corr} = 2 h, 3 colourless chromate on Zn, t_{corr} = 1.5 h.

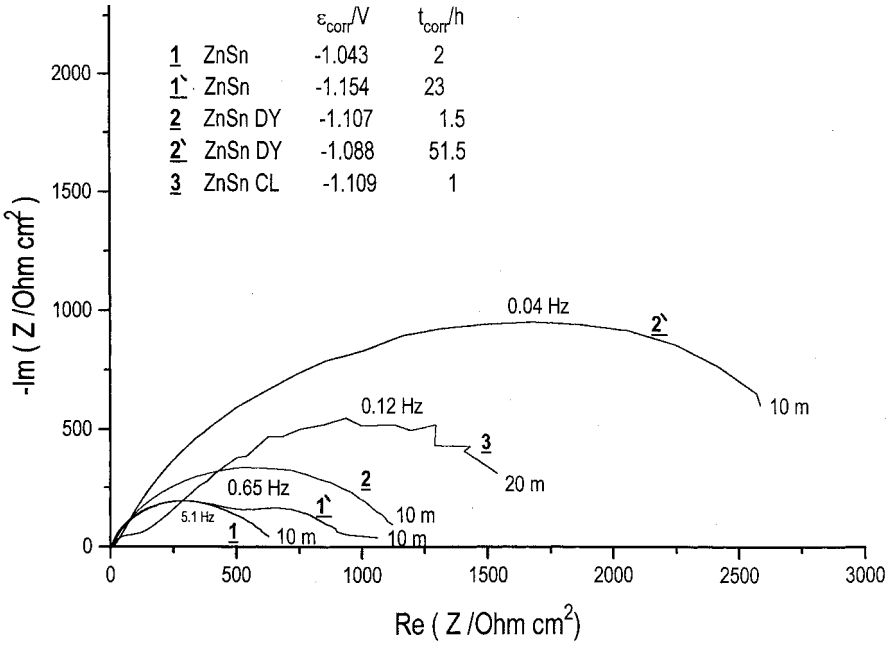

Fig. 4. Complex plane plots of measured impedance spectra of Zn–Sn (20 wt % Sn) deposits with and without chromate layers after immersion into de-aerated 0.5 mol dm^{-3} Na_2SO_4 solution/pH 5, f = 1000 rpm. Key: (1, 1′) Zn–Sn (20 wt %) deposit-2 and 23 h corrosion; (2, 2′) dark yellow chromate on alloy; 1.5 and 51.5 h corrosion; (3) colourless chromate on alloy, 1 h corrosion.

ization resistance (R_p) by the real part of the impedance measured at 10 mHz. The R_p and the appearance of the deposits are collected in Table 2. It is clear that the R_p of the samples increased during the corrosion exposure. However, the opposite effect is observed on the colourless chromate layer either on Zn or Zn–Sn, which dissolved

Table 2. Polarization resistances of various deposits measured by EIS method in deaerated 0.5 mol dm^{-3} Na_2SO_4/pH 5 solution Rotating disc electrodes, $f = 1000$ rpm

Sample	Immersion time /h	ε_c /mV vsSCE	R_p /Ω cm^2	Time /h	ε_c /mV	R_p /Ω cm^2	Appearance after corrosion
Zn	2	−1.066	164	26	−1.081	466	
Zn CL	1.5	−1.079	140	–			dissolved
Zn IY	1	−1.060	565	26	−1.105	1123	partially dissolved removable layer
Zn DY	2	−1.094	1641	–	–	–	partially dissolved removable layer
Zn–Sn	2	−1.043	567	23	−1.154	1022	
Zn–Sn CL	1.5	−1.109	1475	22	−1.016	910	unevenly dissolved
Zn–Sn DY	1.5	−1.107	1061	52	−1.088	2529	uniform removable layer

rapidly. The results of the EDS microanalyses collected in Table 4 exemplify the dezinfication of the colourless chromated alloy, resulting in a very uneven surface. The initial relatively higher R_p can be attributed to tin enrichment during the chromating treatment.

The dark yellow film on Zn initially also gave a higher R_p. The layer dissolved patchily probably due to the discontinuity of the thick nonadherent film (see SEM micrograph, Figure 4 in [7]). Therefore, it may be concluded that the colourless Zn and Zn–Sn and dark yellow Zn chromating films have poor protection ability with prolonged agressive immersion. The corrosion rates were calculated by the Stern–Geary $j_{corr} = B/R_p$ equation, where $B = b_a b_c/2.3\ (b_a + b_c)$. The individual kinetic constants were determined directly at the corrosion potential using the faradaic distortion method, which is known to be applicable for zinc covered by porous oxide layers [1, 12].

Table 3 lists the kinetic constants of some deposits and the corrosion rate calculated from the above equation. The values of the overall kinetic constant B make it evident that due to the change in the corrosion kinetics of the coupled corrosion processes, a reliable corrosion comparison cannot be made by measuring only the polarization resistances. Determination of the corrosion path is also required. The corrosion rate of the DY chromated Zn–Sn deposit after prolonged exposure is only an estimated value in Table 3. In this case the faradaic distortion method was not applicable without interfering with the capacitive current. However, on the basis of the polarization curves shown on Figure 2. it may be assumed that the kinetics are not altered during immersion.

The magnitude of the corrosion rate followed the Zn > Zn–Sn > IY chromated Zn ≃ DY chromated Zn–Sn sequence for short immersion and Zn ≃ Zn − Sn > IY chromated Zn > DY chromated Zn–Sn for prolonged immersion.

The decrease in corrosion rate of the nonchromated Zn–Sn alloy, as compared to pure Zn, is caused by the formation of tin oxides that alter the electrical/electrochemical properties of the corrosion film. We found significant differences in the corrosion kinetics. While the cathodic process on the porous zincoxide/hydroxide layer was activation/mixed controlled, it became diffusion controlled on the alloy, obviously due to the formation of tin oxides. As a consequence of this, the diffusion controlled anodic zinc dissolution changed to charge transfer controlled on the alloy. The elucidation of the semiconducting properties and structure of the oxides formed on the alloy will be the subject of further investigation.

Table 3. Tafel slopes of some deposits measured by faradaic distortion method and corrosion rates in deaerated 0.5 mol dm^{-3} Na_2SO_4/pH 5 solution on rotating disc electrodes, $f = 1000$ rpm

Sample	Immersion time /h	ε_{corr} /V vs SCE	b_a /mV	b_c /mV	B /mV	j_{corr} /μA cm^{-2}
Zn	2	−1.066	33	$-\infty$	14	85
	26	−1.081	34	−241	13	28
Zn IY	2	−1.060	32	−166	12	21
	26	−1.105	33	−166	15	15
Zn–Sn	2	−1.043	62	$-\infty$	27	48
	23	−1.154	71	$-\infty$	30	29
Zn–Sn DY	2	−1.107	67	$-\infty$	29	27
	52	−1.088	–	–	–	< 11

In near neutral 0.5 mol dm^{-3} Na_2SO_4 solution the dark yellow chromate film on Zn–Sn alloy and the iridiscent yellow on Zn yielded the best protective ability in accordance with the conclusions of prolonged salt spray chamber tests [7]. The iridiscent yellow chromate film on Zn is poorly adherent in the dry state and therefore gives a partially dissolved removable layer after aqueous corrosion. The dark yellow chromated Zn–Sn deposit also has a uniform appearance after prolonged corrosion.

3.2. *SEM, TEM investigations on dark yellow chromated Zn–Sn deposits*

The scanning electron microscope pictures of the non-corroded chromated Zn–Sn (~ 20 wt % Sn) samples show a network of cracks on the top of the sample (Figure 5(a)). The microprobe analyses made on these smooth precipitates detected a relatively high Cr content (Table 4), whereas the composition of the polycrystalline grid was nearer to the composition of the original Zn–Sn 20% substrate and it had a smaller chromium content.

The transmission electron microscope study performed on the cross-sectioned samples confirmed the above results. The interface of the chromated layer and the substrate can be seen clearly. The polycrystalline network propagates through the whole chromated layer forming a columnar shape on the cross-sectional electron microscope pictures (Figure 6). According to the electron diffraction analysis, this polycrystalline network consists of ZnO, Zn and Sn crystallites with a small amount of Cr and CrO_3/Cr_2O_3. Between the polycrystalline columns there are smooth areas without any contrast. They correspond to the flakes inside the networks detected by scanning electron microscopy at the top of the chromated sample. Selected area diffraction patterns taken on these places have proved their structure to be amorphous (Figure 6(a, b)). As can be seen on the scanning electron microscope pictures (Figure 5(b)) of the corroded sample, instead of the amorphous flakes, a porous polycrystalline structure appears after corrosion. According to the microprobe analysis, while the Cr content becomes very low (Table 4), the Zn/Sn ratio is nearly the same as in the substrate, but there are light areas with an increased Sn content (Table 4), probably on the locations of the original network. The cross-sectional TEM picture shown in Figure 7(a, b) indicates that the corroded layer is very porous and polycrystalline containing Zn, ZnO and Sn crystallites.

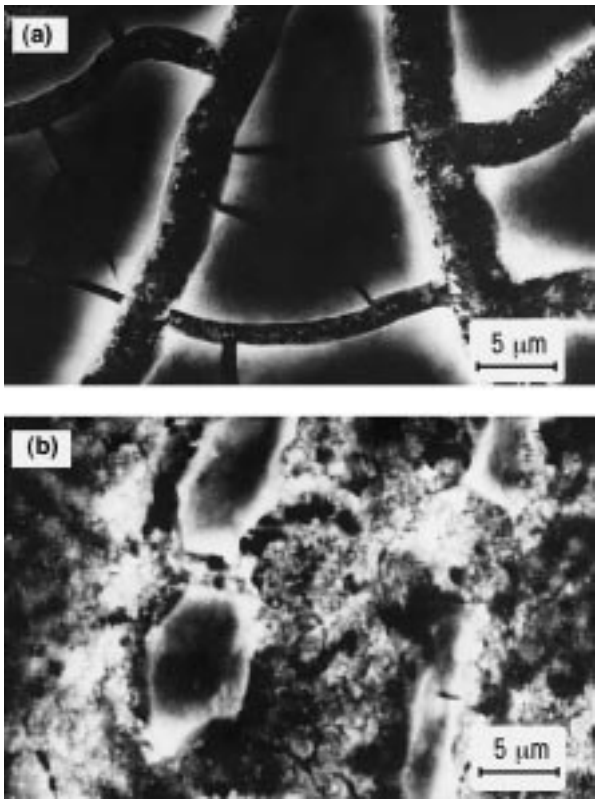

Fig. 5. SEM micrograph of a Zn–Sn (20 wt % Sn) deposit with dark yellow chromate layer. (a) before corrosion, (b) after 6 h corrosion in de-aerated 0.5 mol dm^{-3} Na_2SO_4/pH 5 solution.

Table 4. EDS microprobe analysis of colourless and dark yellow chromated Zn–Sn deposits on selected areas before and after corrosion in deaerated 0.5 mol dm^{-3} Na_2SO_4/pH 5 solution

Composition/wt %		Cr	Sn	Zn	S	Cu	Si
2 Zn–Sn DY noncorroded	on a flake	34–39	11–16	50	–	–	–
	on a groove	6	22	72	–	–	–
2′ Zn–Sn DY corroded for 6 h	on average	3–5	29–82	12–59	0–2	2–9	–
3 Zn–Sn Cl noncorroded	on average	0.32	40.5	56.4	–	2.4	0.4
3′ Zn–Sn corroded for 1.5 h	on spongy area	–	69.4	25	–	5.1	0.6
	on a precipitate	0.3	26.7	71.2	–	1	0.8
	on average	0.4	78.3	17.2	–	3.5	0.6

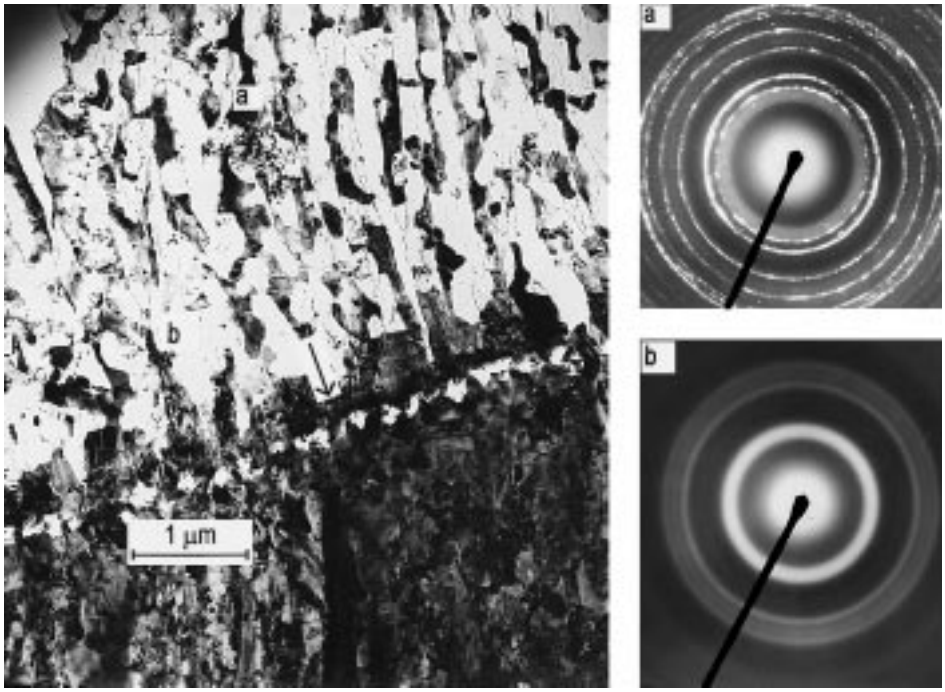

Fig. 6. Electromicrograph and electrondiffraction pattern of a cross-sectioned Zn–Sn (20 wt % Sn) deposit with dark yellow chromate layer before corrosion the arrow shows the transition boundary between the substrate and chromate layer (a) and (b), electon diffraction patterns on selected areas of the chromate layer.

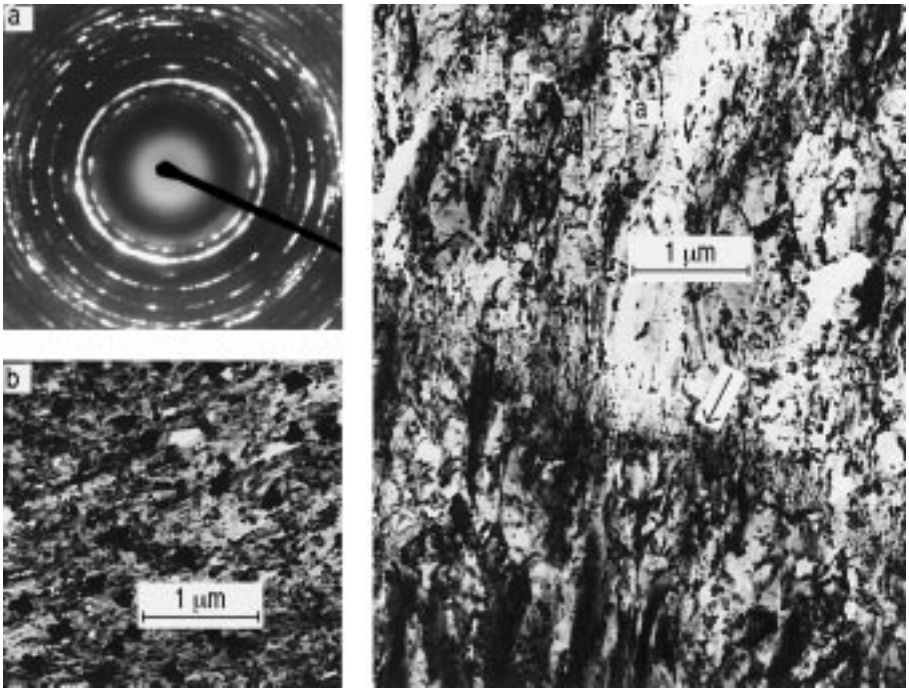

Fig. 7. Electromicrograph and electrondiffraction patterns of a cross-sectioned Zn–Sn (20 wt % Sn) deposit with dark yellow chromate layer after 22 h corrosion the arrows shows the transition layer between the substrate and chromate layer is transformed. (a) Electrondiffraction pattern of the corroded layer, (b) enlargement of the porous chromate layer.

3.3. *XPS analysis of a dark yellow chromated Zn–Sn deposits*

Taking into account the literature data (Table 5) [13, 14] and the XPS spectra of the samples (Figures 8–10) the following compounds are detected in the chromate layer after 6 h aqueous corrosion.

The Cr 2p peaks (Figure 8) after different times of sputtering the samples with Ar^+ are relatively broad indicating that the chromium atoms have more than one chemical state. It is evident (Table 5) that after 1 min sputtering the chromium peak consists of two peaks with binding energies of (i) 578.4 eV, which is characteristic of chromium oxides of the type $ZnCrO_4$ and (ii) 579.8 eV, which corresponds to oxides of six-valent chromium. After a sputtering time of 5 min, the ratio of the six-valent chromium considerably decreases. The subsequent sputterings lead to a peak shape which decomposes into two peaks with binding energies of 577.3 and 578.6 eV, respectively. The former peak is characteristic of an oxide of three-valent chromium and probably, chromium is present not only as $ZnCrO_4$ but also as Cr_2O_3.

After 1 min sputtering, Zn is mainly in sulphate form and there is a pronounced asymmetry at 1022.5 eV due to Zn present in $ZnCrO_4$ and ZnO (Figure 9). With increasing sputtering time, the amount of $ZnSO_4$ strongly decreases. The peak of $ZnCrO_4$ and zinc oxides indicates their increasing amount.

The $Sn3d_{5/2}$ peak intensity (Figure 10) reaches its lowest value after 1 min sputtering time and tin is mainly in the metal state since the peak maximum is at 484.2 eV (Table 5). With increasing sputtering time the tin peak intensity grows and a peak with a maximum at 486.6 eV, typical for SnO + SnO_2 is visible.

Table 6 summarizes the composition of chromate films at various sputtering times. The composition of the non-corroded sample were taken from [8]. The table also shows the chemical composition of a sample corroded 144 h in an unstirred solution. After prolonged immersion the CrO_3 and $ZnCrO_4$ were depleted from the top of the layer, and besides the ZnO, SnO and SnO_2 compounds $Zn_4P_2O_7$, P_2O_5, P appeared in the film.

Figure 11 shows the change of the concentration of detected elements with various times of sputtering by Ar^+. After corrosion, the quantities of O and Zn significantly increase, obviously due to ZnO formation enriching on the top. The P content is almost leached from the film corroding in stirred solution. The amount of Sn/SnO/SnO_2 is slightly higher after corrosion. The amount of chromium, excepting the last layer (about 1.5 nm), is almost invariable due to the corrosion.

Table 5. XPS peak energy assignments, taken from [13] and [14]

Element	Binding energy/eV	Species
Cr 2p	573.5	Cr
	576.8	Cr_2O_3
	578.5	$ZnCrO_4$
	579.8	CrO_3
Zn 2p	1021.6	Zn
	1022.0	ZnO
	1022.5	ZnS
	1023.0	$ZnSO_4$
Sn 3d	484.0	Sn
	486.9	SnO_2
	487.2	SnO
P 2p	135.0–135.6	P_2O_5, P_4O_{10}
	135.3	$Zn_4P_2O_7$

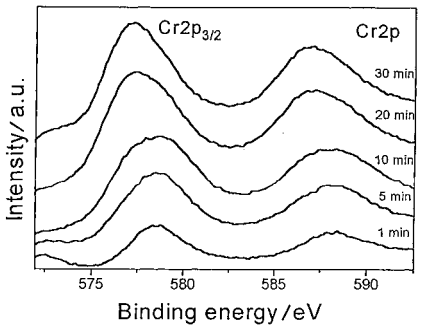

Fig. 8. Cr 2p XPS spectra of a dark yellow chromate layer on Zn–Sn deposit after 6 h corrosion in deaerated 0.5 mol dm^{-3} solution at a sputtering time of 1, 5, 10, 20 and 30 min.

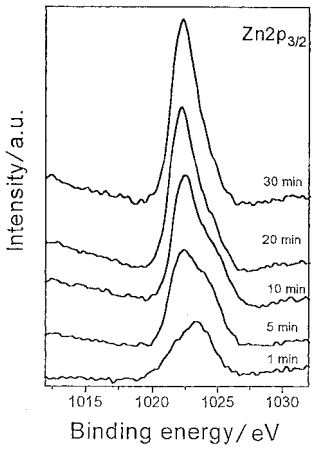

Fig. 9. Zn 2p XPS spectra of a dark yellow chromate layer on Zn–Sn deposit after 6 h corrosion in deaerated 0.5 mol dm^{-3} solution at a sputtering time of 1, 5, 10, 20 and 30 min.

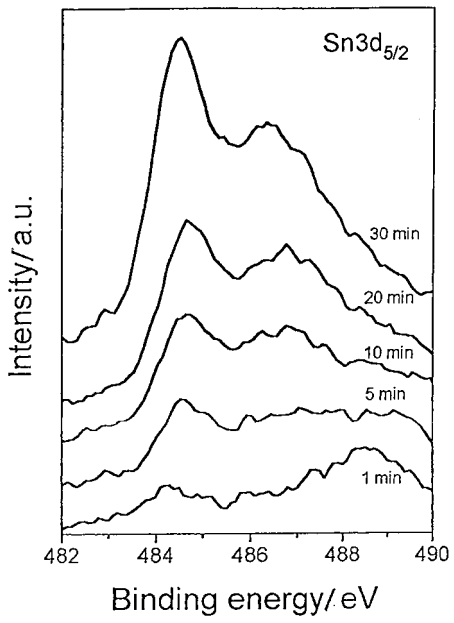

Fig. 10. Sn 3d XPS spectra of a dark yellow chromate layer on Zn–Sn after 6 h corrosion in deaerated 0.5 mol dm^{-3} solution at a sputtering time of 1, 5, 10, 20 and 30 min.

4. Conclusions

Zn and Zn–Sn deposits with and without chromate films were characterized using electrochemical impedance, SEM/TEM and XPS techniques. The corrosion protection offered under aqueous immersion conditions are summarized as follows:

(i) The moderate corrosion rate of Zn–Sn deposits as compared to Zn is attributable to the more compact corrosion layer containing zinc and tin oxides. This corrosion layer alters the anodic control of the corrosion kinetics to cathodic control.

(ii) The iridiscent yellow Zn and dark yellow chromated Zn–Sn have the best corrosion performance, in agreement with the salt spray tests. These chromate films are microcracked, but their corrosion attack is continuous and the formed porous and solution filled chromate layer decreases the corrosion rate.

(iii) The electron micrographs of the cross-sectioned corrosion layers showed that instead of the amorphous precipitates containing CrO_3/Cr_2O_3 compounds, a porous polycrystalline structure with ZnO, Zn and Sn content appears. The XPS results confirmed the chromate layer to be electroactive. Besides the leaching of phosphorous and some chromium compounds, Zn_2CrO_4, $ZnSO_4$, ZnO and SnO/SnO_2 compounds accumulated in the conversion layer. The surface alkalinity due to hydrogen evolution was a possible trap of Zn release by precipitating the zinc and tin oxides. After more prolonged corrosion in unstirred solution greater amounts of $SnO + SnO_2$, $ZnSO_4$ and $Zn_4P_2O_7$ were incorporated in the conversion layer.

(iv) The R_p measurements carried out by a.c. impedance on Zn and Zn–Sn deposits showed that the P-containing dark yellow chromate layer significantly improved the corrosion protection of

Table 6. Composition of passive DY chromate films on Zn–Sn alloy prior to and after corrosion treatment at various sputtering times (ST)

Sputtering time/min	Prior to corrosion treatment	After 6 h corrosion treatment on rotating electrode, f = 1000 rpm	After 144 h corrosion treatment without solution stirring
0	CrO_3, Cr_2O_3, $ZnCrO_4$, ZnO, $Zn_3(PO_4)_2$, SnO_2 + SnO > Sn, P_4O_{10}		
1	$Cr_2O_3 \gg CrO_3$, $ZnCrO_4$, ZnO, SnO_2 + SnO > Sn	$ZnCrO_4$, CrO_3, ZnO, $ZnSO_4$, SnO_2 + SnO > Sn	Cr_2O_3, ZnO, $Zn_3(PO_4)_2$, SnO + SnO_2, $ZnSO_4$, P_2O_5, P_4O_{10}, $Zn_4P_2O_7$
3	$Cr_2O_3 \gg$ ZnCrO4, ZnO, SnO_2 + SnO ≈ Sn		
5		$ZnCrO_4$ > CrO_3, ZnO > $ZnSO_4$, SnO_2 + SnO ≈ Sn	
10	Cr_2O_3, ZnO, Sn > SnO_2 + SnO, P_4O_{10}	Cr_2O_3, $ZnCrO_4$, ZnO, Sn > SnO + SnO_2	$Cr_2O_3 \gg CrO_3$, ZnO, SnO + SnO_2, P_2O_5, P_4O_{10} + $Zn_4P_2O_7$, $ZnSO_4$, ZnS
20		$Cr_2O_3 \gg ZnCrO_4$, ZnO, Sn > SnO	
30		Cr_2O_3, ZnO, Sn ≫ SnO	$Cr_2O_3 \gg CrO_3$, ZnO, SnO + SnO_2, P_2O_5, P_4O_{10} + $Zn_4P_2O_7$, $ZnSO_4$, ZnS
50	Cr_2O_3, ZnO, Zn, Sn ≫ SnO_2 + SnO		

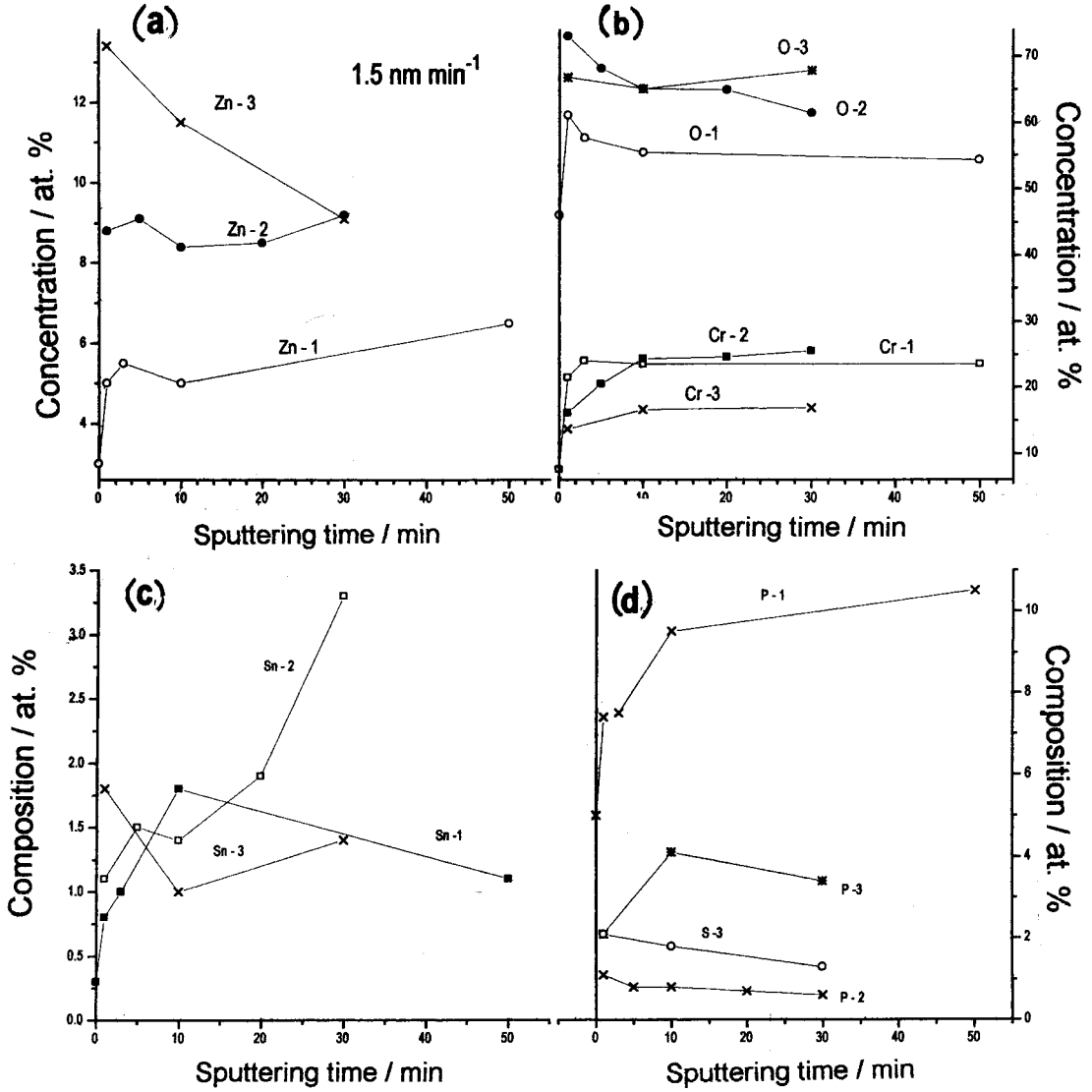

Fig. 11. The in-depth XPS profile of the elemental composition of dark yellow chromate layers on Zn–Sn (20 wt % Sn). Key: (a) for Zn, (b) for Cr and O, (c) for Sn and (d) for P and S. (1) before corrosion, (2) after 6 h corrosion and (3) after 144 h corrosion in deaerated 0.5 mol dm^{-3} Na_2SO_4/pH 5 solution, respectively.

the Zn–Sn deposit. Despite the fact that the chromate layer underwent structural and chemical transformation, the accumulating corrosion product gave better corrosion protection. After repeated drying and immersing, the dark yellow chromated Zn–Sn electrodeposits gave better protection as compared to that of nonchromated deposits.

Acknowledgement

This work was supported by the National Research Fund (OTKA) Under Contract T014959.

References

1. L. Sziráki, H. Csontos, M.L. Varsányi and L. Kiss, *Corros. Sci.* **35** (1993) 371.
2. A. Brenner, *Electrodeposition of Alloys*, Academic Press, New York, vol. 2 (1963) p. 53.
3. G.D. Wilcox and D.R. Gabe, *Corros. Sci.* **35** (1993) 1251.
4. G. Bech-Nielsen and G.D. Juhl, *Corros. Sci.* **34** (1993) 785.
5. E. Budman, Proc. AESF Aerospace Symp., Orlando, FL (29–30 Jan. 1992), p. 129.
6. St. Vitkova, V. Ivanova and G. Raichevsky, *Surf. Coat. Technol.* **82** (1996) 226.
7. V. Ivanova, G. Raichevsky, St. Vitkova and M. Nikolova, *Surf. Coat. Technol.* **82** (1996) 232.
8. G. Raichevsky, V. Ivanova, St. Vitkova and M. Nikolova, *Surf. Coat. Technol.* **82** (1996) 239.

9. J. Dévai and L. Mészáros, *Acta Chim. Acad. Hung.* **100** (1979) 183; L. Mészáros, G. Mészáros and B. Lengyel, *J. Electrochem. Soc.* **141** (1994) 2068.
10. L. Weng, G. Vereecke, M. Genet, P. Berrand and W. Stone, *Surf. Inter. Anal.* **20** (1993) 179.
11. J. Scofield, *J. Electron Spectrosc. Relat Phenom.* **8** (1972) 12.
12. L. Sziráki and L. Kiss, *ACH-Models in Chemistry* **131** (1994) 581.
13. V.I. Nefedov, *Rentgeno-elektroskopija Chemicheskich Soedinenija*, Chimija, Moskow (1984).
14. G.E. Muilenberg (ed.), *Handbook of X-ray Photoelectron Spectroscopy*, Perkin–Elmer Corporation, Physical Electronics Division, MN (1978).